Ultrafast Dynamics of Plasmon-Mediated Charge Transfer in Ag@CeO_2 studied by Free Electron Laser time-resolved X-ray Absorption Spectroscopy

Jacopo Stefano Pelli Cresi[1], Emiliano Principi[1], Eleonora Spurio[2,3], Daniele Catone[4], Patrick O'Keeffe[5], Stefano Turchini[4], Stefania Benedetti[3], Avinash Vikatakavi[2,3], Sergio D'Addato[2,3], Riccardo Mincigrucci[1], Laura Foglia[1], Gabor Kurdi[1], Ivaylo P. Nikolov[1], Giovanni de Ninno[1], Claudio Masciovecchio[1], Jagadesh Kopula Kesavan[6], Federico Boscherini [6] and Paola Luches[3]

[1] Elettra-Sincrotrone Trieste, Strada Statale 14 km 163.5 in Area Science Park, 34012 Basovizza, Trieste, Italy

[2] Dipartimento FIM, Università degli Studi di Modena e Reggio Emilia, Via Campi 213/a, 41125 Modena, Italy.

[3] CNR-NANO, Centro di Ricerca S3, via G. Campi 213/a, 41125 Modena, Italy.

[4] CNR-ISM, Division of Ultrafast Processes in Materials (FLASHit), Area della Ricerca di Roma 2 Tor Vergata, Via del Fosso del Cavaliere 100, 00133 Rome, Italy.

[5] CNR-ISM, Division of Ultrafast Processes in Materials (FLASHit), Area della Ricerca di Roma 1, I-00015 Monterotondo Scalo, Italy

[6] Dipartimento di Fisica e Astronomia, Alma Mater Studiorum – Università di Bologna, Viale C. Berti Pichat 6/2, 40127 Bologna, Italy

Abstract

Expanding the activity of wide band gap semiconductors from the UV into the visible range has become a central goal for the widespread use of these materials in green solar photocatalysis. The hybrid plasmonic/semiconductor system studied here, which is based on silver nanoparticles (Ag NPs) embedded in a film of CeO_2, is an example of a material developed with this aim. In this work, we take advantage of the chemical sensitivity of free electron laser (FEL) time-resolved soft X-ray absorption spectroscopy (TRXAS) to provide information on the ultrafast energy transfer process from the Ag NPs to the CeO_2 film following photoexcitation of the plasmon resonance of the embedded Ag NPs. Ultrafast changes (< 200 fs) of the Ce $N_{4,5}$ absorption edge allowed us to conclude that the initially excited Ag NPs transfer electrons to the Ce atoms of the CeO_2 film by a highly-efficient electron-based mechanism which competes with energy transfer to the lattice of either component of the hybrid material. These results demonstrate the power of FEL-based TRXAS measurements for the characterization of energy transfer in these novel hybrid plasmonic/semiconductor materials.

In recent years, the use of solar light to drive catalytic reactions is becoming a potential green alternative to traditional thermally driven heterogeneous catalysis (*1*). Successful implementation of solar-based photocatalysis in applications such as H_2O splitting and CO_2 reduction would give an important boost to the renewable energy technologies industry (*2*, *3*). Transition metal oxides (TMOs) such as TiO_2, ZnO or CeO_2, have very good catalytic properties, but they exhibit rather poor light-induced activity in the visible range as an effect of their wide bandgap. Several studies have demonstrated that the combination of these materials with plasmonic nanoparticles (NPs) can effectively extend their photoactivity into the visible (*4*–*7*). The strong interaction between metal nanostructures and light

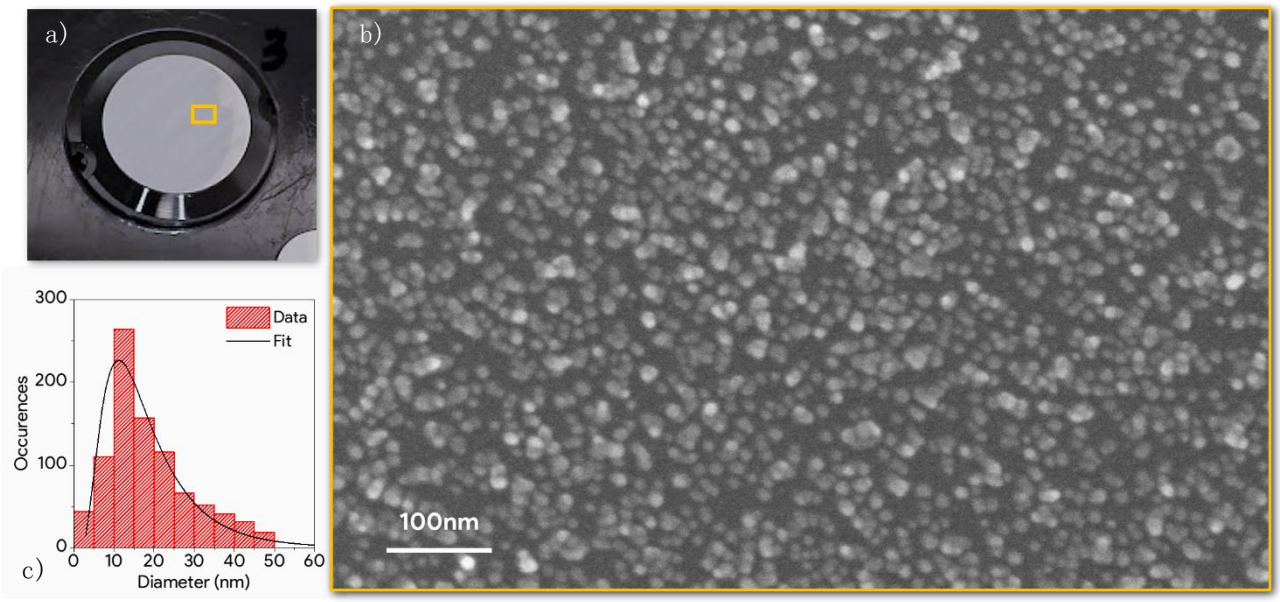

Figure 1 a) Picture of the Ag@CeO2 sample on a parylene substrate; b) SEM image of a sample made of Ag NPs on a CeO2 film grown on a Si substrate; c) Ag NPs size distribution extracted from b.

triggers localized surface plasmon resonances (LSPR) accompanied by an energy and/or charge transfer process from the plasmonic material to the neighboring oxide that boosts the TMO reactivity in the visible range. Moreover, the formation of a Schottky barrier at the interface between the metal and the TMO hinders the fast recombination of the injected electrons (holes), increasing their probability of being involved in redox reactions (*5*).

The LSPR de-excitation can activate the TMO through three main groups of mechanisms (*8*): *i)* electron transfer processes, dominating in the first hundreds of femtoseconds (*9–12*), *ii)* photothermal conversion, prevailing on the picosecond time scale when electron-phonon and phonon-phonon scattering become the dominant channels (*13*, *14*), *iii)* photonic enhancement or electric field enhancement (*15*), which can excite the oxide only for photon energies greater than the band gap and prevails for NP with diameters above a few tens of nm. These specific mechanisms have to be understood and optimized to efficiently exploit the energy/charge transfer processes in the various applications involving solar energy conversion, such as photocatalysis or photovoltaics. This represents a challenging task, which can be achieved by studies of the dynamic evolution of the systems after LSPR excitation.

CeO_2 (cerium oxide or ceria) plays an important role as a TMO catalyst material. Its electronic configuration, with a bandgap in the ultraviolet range (3.2 – 4.0 eV) (*16*, *17*), allows fast and reversible changes between the most stable 4+ oxidation state and the 3+ oxidation state of Ce with one extra electron localized in the Ce 4f levels between the filled valence band and the empty conduction band. This property is associated with the remarkable capability of ceria to store, transport and release oxygen depending on the environmental conditions. The combination of ceria with plasmonic NPs induces modifications of important properties, such as oxygen vacancy formation energy, which may improve the material reactivity. An increase of the sensitivity of Ag NPs/CeO_2 systems to visible light has been recently highlighted (*18–20*), however the mechanisms involved in the LSPR-mediated enhancement remain poorly understood. Recent experiments, carried out on a UV/Vis time-resolved facility on the Ag

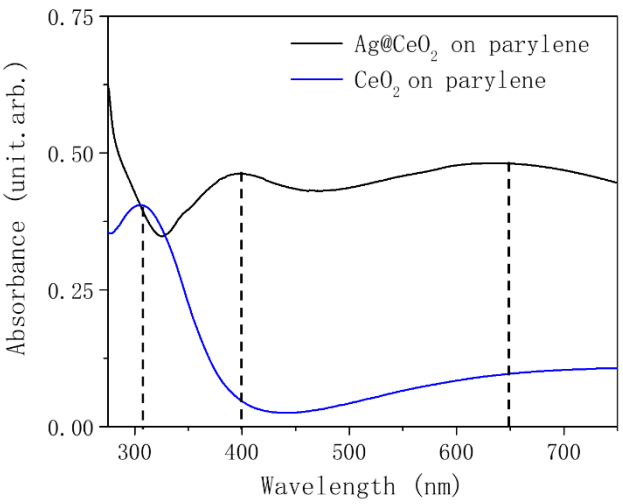

Figure 2 Absorbance spectra of the Ag@CeO_2 film (black), and of a ceria film (blue).

NPs/CeO_2 system (*4*), revealed a potential electron transfer process from NPs to the oxide occurring on the sub-picosecond time scale. In general, ultrafast spectroscopies in the ultraviolet, visible and infrared range, lack of chemical sensitivity (*4*, *21*) thus limiting the interpretation of the results to qualitative considerations.

X-ray absorption spectroscopies (XAS) represent a valuable tool to obtain element-specific information on light-triggered ultrafast processes, providing very high sensitivity to the fine details of the electronic structure of the individual elements present in the investigated materials (*22*). Ultrashort pulses (from fs to hundreds of fs) of soft x-rays can be generated by both free-electron laser (FEL) and high harmonic generation sources. FEL sources are particularly suitable for ultrafast core-level spectroscopies as they guarantee high pulse intensities in a rather large spectral range. In particular, the FERMI FEL in Trieste (Italy) gives the possibility of finely tuning the photon energy within the 20-300 eV photon energy range, guaranteeing a remarkable spectral stability and nearly transform-limited pulses (*23*). These features, accompanied by an almost jitter-free laser-FEL synchronization (*24*), are ideal for laser pump-X-ray probe single-shot experiments. In this work, we carry out a time-resolved XAS experiment on a light activated Ag NPs/CeO_2 sample with the aim of exploring the ultrafast changes occurring in the electronic structure of Ce and finally shedding light on the nature of the charge transfer from Ag NPs to CeO_2 following LSPR excitation.

The Ag NPs/CeO_2 samples employed in this study were grown at the SESAMo laboratories in Modena on ultrathin (100 nm) parylene-N self-standing foils, as soft X-ray transparent substrates. Mass-selected Ag NPs, with an average diameter *d* of ~10 nm (Fig. 1), were grown by an inert gas aggregation cluster source based on magnetron sputtering. The NPs were co-evaporated with cerium oxide forming a film with embedded NPs, hereafter referred to as Ag@CeO_2 (*4*). This specific configuration is considered better than the CeO_2-supported Ag NPs scheme, as it maximizes the interface region, where the metal-oxide interaction takes place, and protects the Ag NPs from contamination. A cerium oxide film of the same thickness without Ag NPs was also grown for reference. The samples were characterized by X-ray photoelectron spectroscopy in-situ (see Supporting Information) and transferred under inert atmosphere to the experimental setups for optical, XAS and time-resolved XAS characterization.

The samples were preliminary characterized using steady UV-Vis spectrophotometry, to verify the response of the Ag@CeO_2 system to visible light and to identify the spectral features of Ag NPs and CeO_2. The spectra, in Fig. 2, show that the absorbance of the ceria film without Ag NPs exhibits a peak at 300 nm (blue line). This spectral feature is compatible with excitations from the valence band to empty 4f levels, in agreement with the literature (*16*, *17*). The Ag@CeO_2 sample shows broad and intense absorbance peaks centered at 400 nm and 650 nm, ascribed to the LSPR excitation of Ag NPs. The specific

origin of the two peaks was investigated through simulations of the absorbance of Ag NPs in a CeO_2 matrix, performed using the boundary element method, as implemented in the MNPBEM17 toolbox (*25*). The simulations show that the peaks can be ascribed to different specific configurations of the Ag NPs within the CeO_2 matrix and to extended plasmon resonances introduced by the proximity of the NPs (details in the Supporting Information).

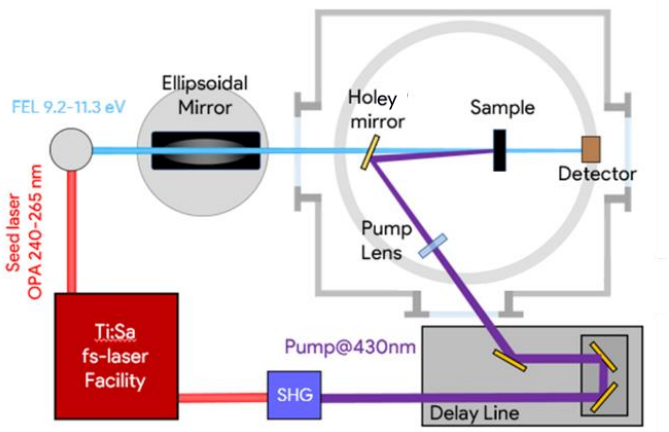

Figure 3 EIS-TIMEX end-station setup for pump-probe XAS measurements in transmission geometry. Small angles between pump and FEL are achieved using a holey steering mirror positioned in the FEL beam path. Synchronization between the laser pump and FEL probe is nearly jitter-free being both the pulses generated by the same Ti:Sa oscillator.

Stationary XAS spectra of the samples at the Ce $N_{4,5}$ edge have been carried out at the BEAR beamline of ELETTRA (*26*) for reference. Figure 4 shows the reference spectra for the CeO_2 film and the Ag@CeO_2 sample after pre-edge background subtraction (red and black solid lines respectively). The spectrum of the CeO_2 film is compatible with the Ce^{4+} reference spectrum reported in the literature (*27*), shown as a dashed green line in Figure 4. The addition of Ag NPs in the CeO_2 system induces a red-shift of about 1eV of the Ce absorption edge and a tangible decrease of the white line height. Both effects are compatible with a mild reduction of cerium oxide in the Ag@CeO_2. A more pronounced reduction of the oxide in the Ag@CeO_2 sample is expected to lead to a spectral shape more similar to the Ce^{3+} reference spectrum (*27*) (dashed blue line). The mild reduction in Ag@CeO_2 is confirmed by x-ray photoemission spectroscopy measurements (see Figure S2, Supporting Information) and it results from electron transfer from Ag NPs to the oxide (*28*, *29*) typical of metal NP/oxide systems.

The TRXAS measurements have been performed at the EIS-TIMEX end-station (*30*) of the FERMI FEL (Trieste, Italy) operating in single-shot laser pump-FEL probe mode (Fig. 3) on the Ag@CeO_2 sample at selected energies across the Ce $N_{4,5}$-edge. An ultrashort laser pulse at 430 nm is used as a pump to selectively excite the Ag NPs LSPR. Indeed, the optical absorption of CeO_2 matrix is negligible at the pump photon energy if compared to the Ag NPs one (see Figure 2). Four specific FEL photon energies (119 eV, 122 eV, 130 eV and 133 eV), marked by the purple arrows in Figure 4, were chosen to maximize the sensitivity to possible changes in the electronic structure in Ce ions driven by ultrafast reduction of CeO_2. The FEL and the laser pump beam diameters on the sample were 80 and 100 µm, respectively. The pump pulse duration was estimated to be about 200 fs, while the average FEL probe pulse duration was around 100 fs. The instrument response function (IRF) of the setup is thus dominated by the pump laser duration. The laser pump fluence was set to about 34 mJ cm^{-2}. The TRXAS measurements were performed in the transmission mode by rastering the sample in the plane perpendicular to the beam and illuminating fresh regions of the sample at each pump shot. Transmission of the unperturbed sample in every fresh position was measured by exposing the sample to a sequence of probe pulses prior to pump exposure. The delay time between the pump and the probe pulses was scanned with steps of 0.1 ps within

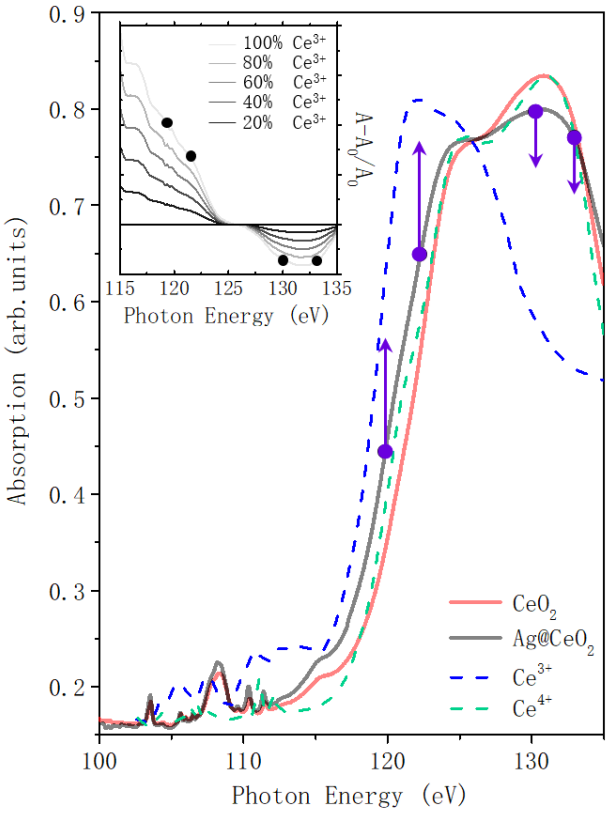

Figure 4 Ce N_{45} XAS absorption spectra measured in transmission mode for CeO_2 (solid red line) and Ag@CeO_2 (solid black line) samples. The spectra of Ce^{4+} (dashed green line) and Ce^{3+} (dashed blue line) reference samples taken from the literature (*26*) are also reported. The inset reports the relative variation of absorption during the reduction of Ce (Ce^{4+}→Ce^{3+}). Purple arrows indicate the selected FEL energies used to probe the variations of absorption.

a range of about 1 ps from their overlap time. Repeated single-shot measurements at each delay time in different positions have been carried out on the sample, thus obtaining good counting statistics for each chosen photon energy. In order to account for possible non-uniformities of the sample, we have neglected the first and the last ventile in the distribution of the measured changes in transmission for each energy and delay.

Figure 5 reports the variation of the absorption, as a function of the pump-probe delay time, at the selected FEL photon energies across the Ce $N_{4,5}$-edge. In particular, the X-ray absorption coefficient after excitation exhibits a pronounced increase at 119 eV and 122 eV of about 10% (Figure 5 a and b) and a decrease at 130 eV and 133 eV of about 5% (Figure 5 c and d).

The changes in the X-ray absorption occur within the first few hundreds of fs and persist at least up to about 1ps delay time between the pump and the probe. The inset of Figure 4 shows the expected relative absorption changes of Ce N_{45} XAS spectra if the electronic configuration of Ce is progressively modified by adding electrons in the 4f levels (calculated using the reference spectra and assuming different concentrations of Ce^{3+}). A pronounced increase of absorption below 125 eV and a moderate decrease above 125 eV are expected with increasing concentration of Ce^{3+} ions, in agreement with TRXAS findings. Therefore, the absorption change shown in Fig. 5 appears to be compatible with an ultrafast reduction of part of the Ce ions in the sample, driven by a LSPR-mediated electron injection in the Ce 4f localized states of the CeO_2 surrounding the Ag NPs.

The data in Figure 5 were fit using a kinetic profile (obtained by the product of an exponential functions and a step function) convoluted with an IRF of Gaussian shape with FWHM of 200 fs, compatible with the width of the pump laser. The results of the fit show that the rise time of the signal is compatible with the pump pulse duration. This evidence confirms that the charge transfer process is faster than a typical thermal process (electron-phonon scattering), which requires typical rising times of 1-10 ps (*31*, *32*). The negligible decay of the transient XAS signal at long delay times up to 1 ps is consistent with the long-lived excited state that we observed in previous experiments using a visible probe (*4*) and suggests that the charge injected in 4f states does not recombine rapidly. The amplitude of the observed absorption

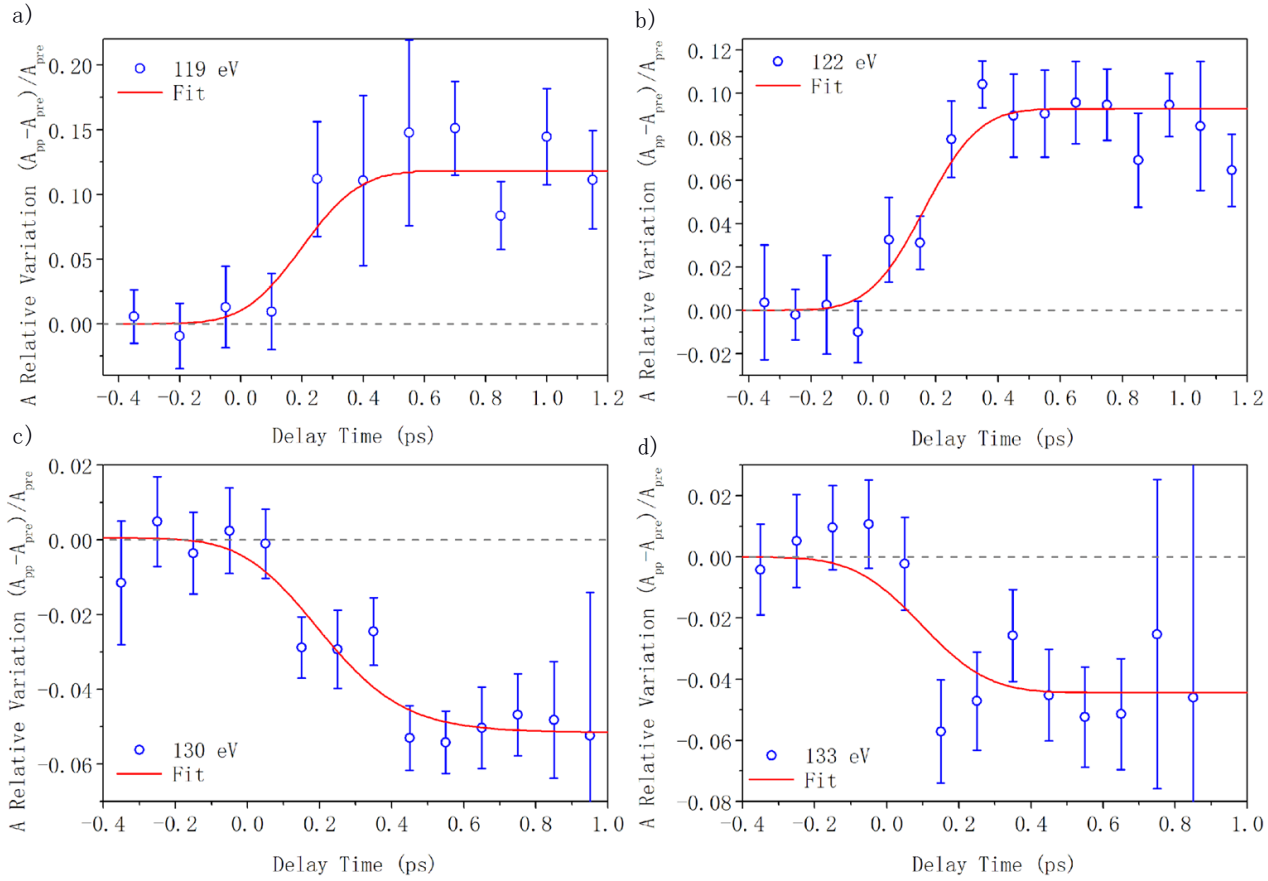

Figure 5 Relative variation of absorption as a function of pump-probe delay time and corresponding fit (red curve) b 122 eV c 130 eV d 133 eV.

variations, estimated by the fit, can be related to the density of electrons transferred to ceria. Using the reference spectra of Ce^{3+} and Ce^{4+} samples (*27*), we related the measured variations in absorption at the different probe energies to the fraction of Ce ions affected by injected electrons. The resulting fraction, estimated in about 20%, indicates that charge transfer does not involve only the cerium atoms contained in the volume of the interfacial cerium oxide layer which surrounds the Ag NPs (see Supporting Information for details). This estimate allows us to infer a high efficiency for the plasmon-mediated electron transfers and it suggests that by combining Ag NPs with ultrathin oxide shells the plasmon-induced oxide excitation can be maximized.

The experiment described here is the first application of FEL-based time-resolved XAS to a hybrid plasmonic NPs/oxide material for photocatalysis. The TRXAS measurements presented reveal for the first time that the electronic structure of the Ce atoms undergoes an ultrafast change following photoexcitation of the LSPR of the Ag NPs. The sign and the amplitude of the observed changes at the different energies and their ultrafast nature demonstrate that the decay of LSPR in the Ag NPs involves electron transfer processes, which dominate below 1 ps. We believe that this experiment will open the photocatalytic material topic to FEL-based investigations. Important advances could be achieved by the use of shorter pulses, to study electron transfer dynamics on a time scale of tens of fs, as well as by the use of different system architectures to maximize the visible-light-induced excitation.

Bibliography

1. H. A. Atwater, A. Polman, Plasmonics for improved photovoltaic devices. *Nature Materials*. **9**, 205–213 (2010).
2. C. Gomes Silva, R. Juárez, T. Marino, R. Molinari, H. García, Influence of Excitation Wavelength (UV or Visible Light) on the Photocatalytic Activity of Titania Containing Gold Nanoparticles for the Generation of Hydrogen or Oxygen from Water. *J. Am. Chem. Soc.* **133**, 595–602 (2011).
3. W. Hou, W. H. Hung, P. Pavaskar, A. Goeppert, M. Aykol, S. B. Cronin, Photocatalytic Conversion of CO2 to Hydrocarbon Fuels via Plasmon-Enhanced Absorption and Metallic Interband Transitions. *ACS Catal.* **1**, 929–936 (2011).
4. J. S. P. Cresi, M. C. Spadaro, S. D'Addato, S. Valeri, S. Benedetti, A. di Bona, D. Catone, L. D. Mario, P. O'Keeffe, A. Paladini, G. Bertoni, P. Luches, Highly efficient plasmon-mediated electron injection into cerium oxide from embedded silver nanoparticles. *Nanoscale* (2019), doi:10.1039/C9NR01390C.
5. L. V. Besteiro, X. T. Kong, Z. Wang, G. Hartland, A. O. Govorov, Understanding Hot-Electron Generation and Plasmon Relaxation in Metal Nanocrystals: Quantum and Classical Mechanisms. *ACS Photonics*. **4**, 2759–2781 (2017).
6. Z. Xu, Y. Lin, M. Yin, H. Zhang, C. Cheng, L. Lu, X. Xue, H. J. Fan, X. Chen, D. Li, Understanding the Enhancement Mechanisms of Surface Plasmon-Mediated Photoelectrochemical Electrodes: A Case Study on Au Nanoparticle Decorated TiO2 Nanotubes. *Advanced Materials Interfaces*. **2**, 1500169 (2015).
7. Y.-H. Chiu, K.-D. Chang, Y.-J. Hsu, Plasmon-mediated charge dynamics and photoactivity enhancement for Au-decorated ZnO nanocrystals. *Journal of Materials Chemistry A*. **6**, 4286–4296 (2018).
8. C. Zhan, X.-J. Chen, J. Yi, J.-F. Li, D.-Y. Wu, Z.-Q. Tian, From plasmon-enhanced molecular spectroscopy to plasmon-mediated chemical reactions. *Nature Reviews Chemistry*. **2**, 216–230 (2018).
9. R. Long, O. V. Prezhdo, Instantaneous generation of charge-separated state on TiO2 surface sensitized with plasmonic nanoparticles. *Journal of the American Chemical Society*. **136**, 4343–4354 (2014).
10. T. P. White, K. R. Catchpole, Plasmon-enhanced internal photoemission for photovoltaics: Theoretical efficiency limits. *Applied Physics Letters*. **101**, 073905 (2012).
11. S. Tan, A. Argondizzo, J. Ren, L. Liu, J. Zhao, H. Petek, Plasmonic coupling at a metal/semiconductor interface. *Nature Photonics*. **11**, 806–812 (2017).
12. A. O. Govorov, H. Zhang, Y. K. Gun'Ko, Theory of photoinjection of hot plasmonic carriers from metal nanostructures into semiconductors and surface molecules. *Journal of Physical Chemistry C*. **117**, 16616–16631 (2013).
13. J. Cao, T. Sun, K. T. V. Grattan, Gold nanorod-based localized surface plasmon resonance biosensors: A review. *Sensors and Actuators, B: Chemical*. **195**, 332–351 (2014).
14. Y. Dubi, I. Wai Un, Y. Sivan, Thermal effects – an alternative mechanism for plasmon-assisted photocatalysis. *Chemical Science*. **11**, 5017–5027 (2020).
15. J. Li, S. K. Cushing, P. Zheng, F. Meng, D. Chu, N. Wu, Plasmon-induced photonic and energy-transfer enhancement of solar water splitting by a hematite nanorod array. *Nature Communications*. **4**, 2651 (2013).
16. P. Patsalas, S. Logothetidis, L. Sygellou, S. Kennou, Structure-dependent electronic properties of nanocrystalline cerium oxide films. *Phys. Rev. B*. **68**, 035104 (2003).
17. J. S. Pelli Cresi, L. Di Mario, D. Catone, F. Martelli, A. Paladini, S. Turchini, S. D'Addato, P. Luches, P. O'Keeffe, Ultrafast Formation of Small Polarons and the Optical Gap in CeO2. *J. Phys. Chem. Lett.* **11**, 5686–5691 (2020).
18. M. Kazazi, B. Moradi, M. D. Chermahini, Enhanced photocatalytic degradation of methyl orange using Ag/Sn-doped CeO 2 nanocomposite. *Journal of Materials Science: Materials in Electronics*. **30** (2019), pp. 6116–6126.

19. P. Verma, Y. Kuwahara, K. Mori, H. Yamashita, Plasmonic catalysis of Ag nanoparticles deposited on CeO2 modified mesoporous silica for the nitrostyrene reduction under light irradiation conditions. *Catalysis Today*. **324**, 83–89 (2019).

20. J. S. Pelli Cresi, E. Silvagni, G. Bertoni, M. C. Spadaro, S. Benedetti, S. Valeri, S. D'Addato, P. Luches, Optical and electronic properties of silver nanoparticles embedded in cerium oxide. *J. Chem. Phys.* **OXIDE2020**, 114704 (2020).

21. D. C. Ratchford, A. D. Dunkelberger, I. Vurgaftman, J. C. Owrutsky, P. E. Pehrsson, Quantification of Efficient Plasmonic Hot-Electron Injection in Gold Nanoparticle–TiO2 Films. *Nano Letters*. **17**, 6047–6055 (2017).

22. F. Boscherini, in *X-Ray Absorption Spectroscopy of Semiconductors* (Springer, 2014).

23. E. Allaria, D. Castronovo, P. Cinquegrana, P. Craievich, M. Dal Forno, M. B. Danailov, G. D'Auria, A. Demidovich, G. De Ninno, S. Di Mitri, B. Diviacco, W. M. Fawley, M. Ferianis, E. Ferrari, L. Froehlich, G. Gaio, D. Gauthier, L. Giannessi, R. Ivanov, B. Mahieu, N. Mahne, I. Nikolov, F. Parmigiani, G. Penco, L. Raimondi, C. Scafuri, C. Serpico, P. Sigalotti, S. Spampinati, C. Spezzani, M. Svandrlik, C. Svetina, M. Trovo, M. Veronese, D. Zangrando, M. Zangrando, Two-stage seeded soft-X-ray free-electron laser. *Nature Photonics*. **7**, 913–918 (2013).

24. M. B. Danailov, F. Bencivenga, F. Capotondi, F. Casolari, P. Cinquegrana, A. Demidovich, E. Giangrisostomi, M. P. Kiskinova, G. Kurdi, M. Manfredda, C. Masciovecchio, R. Mincigrucci, I. P. Nikolov, E. Pedersoli, E. Principi, P. Sigalotti, Towards jitter-free pump-probe measurements at seeded free electron laser facilities. *Opt. Express, OE.* **22**, 12869–12879 (2014).

25. U. Hohenester, A. Trügler, MNPBEM - A Matlab toolbox for the simulation of plasmonic nanoparticles. *Computer Physics Communications*. **183**, 370–381 (2012).

26. L. Pasquali, A. De Luisa, S. Nannarone, The UHV Experimental Chamber For Optical Measurements (Reflectivity and Absorption) and Angle Resolved Photoemission of the BEAR Beamline at ELETTRA. *AIP Conference Proceedings*. **705**, 1142–1145 (2004).

27. S. O. Kucheyev, B. J. Clapsaddle, Y. M. Wang, T. van Buuren, A. V. Hamza, Electronic structure of nanoporous ceria from x-ray absorption spectroscopy and atomic multiplet calculations. *Phys. Rev. B.* **76**, 235420 (2007).

28. P. Luches, F. Pagliuca, S. Valeri, F. Illas, G. Preda, G. Pacchioni, Nature of Ag Islands and Nanoparticles on the CeO \textlesssub\textgreater2\textless/sub\textgreater (111) Surface. *The Journal of Physical Chemistry C*. **116**, 1122–1132 (2012).

29. F. Benedetti, P. Luches, M. C. Spadaro, G. Gasperi, S. Daddato, S. Valeri, F. Boscherini, Structure and morphology of silver nanoparticles on the (111) surface of cerium oxide. *Journal of Physical Chemistry C*. **119**, 6024–6032 (2015).

30. C. Masciovecchio, A. Battistoni, E. Giangrisostomi, F. Bencivenga, E. Principi, R. Mincigrucci, R. Cucini, A. Gessini, F. D'Amico, R. Borghes, M. Prica, V. Chenda, M. Scarcia, G. Gaio, G. Kurdi, A. Demidovich, M. B. Danailov, A. D. Cicco, A. Filipponi, R. Gunnella, K. Hatada, N. Mahne, L. Raimondi, C. Svetina, R. Godnig, A. Abrami, M. Zangrando, EIS: the scattering beamline at FERMI. *Journal of Synchrotron Radiation*. **22**, 553–564 (2015).

31. S. Link, M. A. El-Sayed, Spectral Properties and Relaxation Dynamics of Surface Plasmon Electronic Oscillations in Gold and Silver Nanodots and Nanorods. *J. Phys. Chem. B.* **103**, 8410–8426 (1999).

32. A. Furube, L. Du, K. Hara, R. Katoh, M. Tachiya, Ultrafast plasmon-induced electron transfer from gold nanodots into TiO2 nanoparticles. *Journal of the American Chemical Society*. **129**, 14852–14853 (2007).